

Spectral Compressive Imaging Reconstruction Using Convolution and Contextual Transformer

Lishun Wang^{1,2}, Zongliang Wu³, Yong Zhong^{1,2} and Xin Yuan³

¹ Chengdu Institute of Computer Application Chinese Academy of Sciences,

² University of Chinese Academy of Sciences,

³ Westlake University

Abstract

Spectral compressive imaging (SCI) is able to encode the high-dimensional hyperspectral image to a 2D measurement, and then uses algorithms to reconstruct the spatio-spectral data-cube. At present, the main bottleneck of SCI is the reconstruction algorithm, and the state-of-the-art (SOTA) reconstruction methods generally face the problem of long reconstruction time and/or poor detail recovery. In this paper, we propose a novel hybrid network module, namely CCoT (Convolution and Contextual Transformer) block, which can acquire the inductive bias ability of convolution and the powerful modeling ability of transformer simultaneously, and is conducive to improving the quality of reconstruction to restore fine details. We integrate the proposed CCoT block into deep unfolding framework based on the generalized alternating projection algorithm, and further propose the GAP-CCoT network. Finally, we apply the GAP-CCoT algorithm to SCI reconstruction. Through the experiments of extensive synthetic and real data, our proposed model achieves higher reconstruction quality ($>2\text{dB}$ in PSNR on simulated benchmark datasets) and shorter running time than existing SOTA algorithms by a large margin. The code and models are publicly available at <https://github.com/ucaswangls/GAP-CCoT>.

1. Introduction

Hyperspectral image is a spatio-spectral data-cube composed of many narrow spectral bands, with each one corresponding to one wavelength. Compared with RGB images, hyperspectral images have rich spectral information and can be widely used in medical diagnosis [39], food safety [12], remote sensing [4] and other fields. However, existing hyperspectral cameras have a long imaging time and high hardware costs, which greatly limits the application of these hyperspectral cameras. To address the above

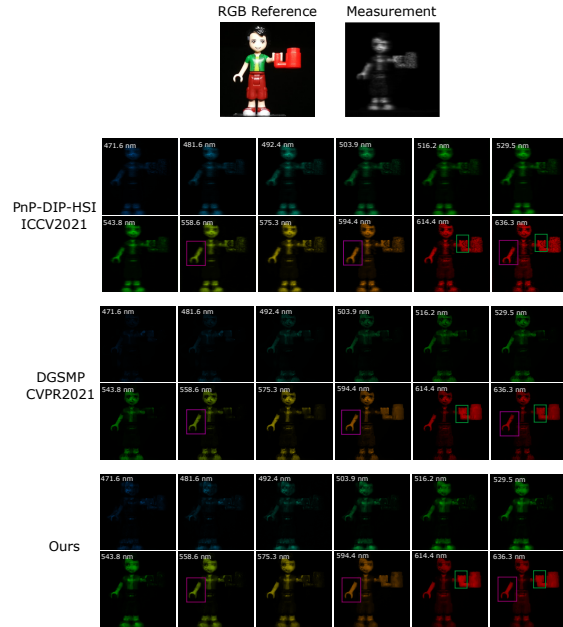


Figure 1. Reconstructed real data of Legoman, captured by the spectral SCI systems in [37]. We show the reconstruction results of 12 spectral channels, and compare our proposed method with the latest self-supervised method (PnP-DIP-HSI [40]) and method based on the Maximum a Posterior (MAP) estimation (DGSMPCVPR2021 [24]). As can be seen from the purple and green areas in the plot, the image reconstructed by our method is clearer, the PnP-DIP-HSI method produced some artifacts, and the DGSMPCVPR2021 method lost some details.

problems, spectral compressive imaging (SCI), especially the coded aperture snapshot spectral imaging (CASSI) system [15,39,53] provides an elegant solution, which can capture the information of multiple spectral bands at the same time with only one two-dimensional (2D) sensor. CASSI uses a physical mask and a prism to modulate the spectral data-cube, and captures the *modulated (and thus compressed) measurement* on the 2D plane sensor. Then recon-

struction algorithms are employed to recover the hyperspectral data-cube from the measurement along with the mask. This paper focuses on the reconstruction algorithm.

At present, SCI reconstruction algorithms mainly include model-based methods and learning-based methods. The traditional model-based methods have relevant theoretical proof and can be explained. The representative algorithms are mainly TwIST [3], GAP-TV [64] and De-SCI [33]. However, model-based methods require prior knowledge, long reconstruction time and usually can only provide poor reconstruction quality. With its strong fitting ability, deep learning model can directly learn relevant knowledge from data and provide excellent reconstruction results [2, 14, 41, 54]. However, compared with the model-based method, the learning-based method lacks interpretability [65].

The deep unfolding network combines the advantages of model-based and learning-based methods, and thus it is powerful with a clear interpretability [16, 60, 61, 68]. At present, most advanced reconstruction algorithms [37, 55] are based on the idea of deep unfolding. Many models combine U-net [46] network with deep unfolding idea for image reconstruction and achieve good reconstruction results. However, the U-net model is too simple to fully obtain the effective information of the image. Therefore, we use the inductive bias ability of convolution and the powerful modeling ability of transformer [17] to design a *parallel module* to solve the problem of SCI reconstruction. As shown in Fig. 1, the integration of our proposed method and the deep unfolding idea can recover more details with fewer artifacts. Our main contributions in this paper are summarized as follows:

- We first apply **transformer into deep unfolding** for SCI reconstruction.
- We propose an effective **parallel network structure composed of convolution and transformer**, dubbed CCoT, which can obtain more effective spectral features.
- Experimental results on a large amount of synthetic and real data show that our proposed method **achieves state-of-the-art (SOTA) results** in the SCI reconstruction.
- The proposed can also **be used in other compressive sensing (CS) systems**, such as video CS [21, 35, 44], and leads to excellent results.

2. Related Work

In this section, we first review the forward model of CASSI, then the existing reconstruction methods are briefly introduced. Focusing the deep learning based models, we

describe the pros and cons of CNN and introduce the visual transformer for other tasks.

2.1. Mathematical Model of SCI System

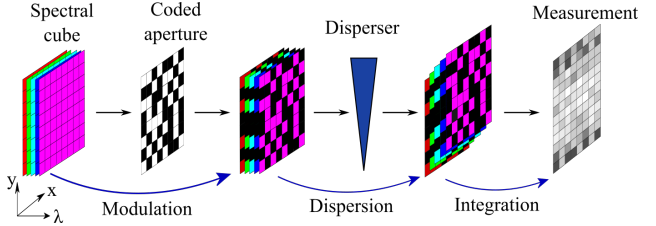


Figure 2. Schematic diagrams of CASSI system.

The SCI system encodes high-dimensional spectral data-cube into a 2D measurement, and the CASSI [53] is one of the earliest SCI systems. As shown in Fig. 2, the three-dimensional (3D) spatio-spectral data-cube is first modulated through a coded aperture (a.k.a., mask). Then, the encoded 3D spectral data-cube is dispersed by the dispersion prism. Finally, the whole spectral dimension data is captured by a 2D camera sensor by integrating across the spectral dimension.

Let $\mathbf{X}^0 \in \mathbb{R}^{n_x \times n_y \times n_\lambda}$ denotes the captured 3D spectral data-cube, $\mathbf{M} \in \mathbb{R}^{n_x \times n_y}$ denotes a pre-defined mask. For each wavelength $m = 1, \dots, n_\lambda$, the spectral image is modulated, and we can express it as

$$\mathbf{X}'(:, :, m) = \mathbf{X}(:, :, m) \odot \mathbf{M}, \quad (1)$$

where $\mathbf{X}' \in \mathbb{R}^{n_x \times n_y \times n_\lambda}$ denotes the modulated spectral data-cube, $\mathbf{X}(:, :, m)$ denotes the m -th channel of the 3D spectral data-cube \mathbf{X} , and \odot denotes the element-wise multiplication.

After passing the dispersive prism, the modulated spectral data-cube is tilted, and the tilted spectral data-cube $\mathbf{X}''(u, v, m) \in \mathbb{R}^{n_x \times (n_y + n_\lambda - 1) \times n_\lambda}$ can be expressed as

$$\mathbf{X}''(u, v, m) = \mathbf{X}'(x, y + d(\lambda_m - \lambda_c), m), \quad (2)$$

where (u, v) represents the coordinate system of the camera detector plane, λ_m represents the wavelength of the m -th channel, λ_c represents the center wavelength, and $d(\lambda_m - \lambda_c)$ represents the spatial shifting of the m -th channel. Finally, by compressing the spectral domain, the camera sensor captures a 2D compressed measurement $\mathbf{Y} \in \mathbb{R}^{n_x \times (n_y + n_\lambda - 1)}$, which can be expressed as

$$\mathbf{Y} = \sum_{m=1}^{n_\lambda} \mathbf{X}''(:, :, m) + \mathbf{Z}, \quad (3)$$

where \mathbf{Z} denotes the measurement noise.

For the sake of simple notations, as derived in [40], we further give the vectorized formulation expression of Eq.

(3). Firstly, we define $\text{vec}(\cdot)$ as vectorization operation of matrix. Then we vectorize

$$\mathbf{y} = \text{vec}(\mathbf{Y}) \in \mathbb{R}^{n_x(n_y+n_\lambda-1)}, \quad (4)$$

$$\mathbf{z} = \text{vec}(\mathbf{Z}) \in \mathbb{R}^{n_x(n_y+n_\lambda-1)}, \quad (5)$$

$$\mathbf{x} = [\mathbf{x}_1^\top, \dots, \mathbf{x}_{n_\lambda}^\top]^\top \in \mathbb{R}^{n_x n_y n_\lambda}, \quad (6)$$

where $\mathbf{x}_m = \text{vec}(\mathbf{X}(:, :, m))$, $m = 1, \dots, n_\lambda$. In addition, we define sensing matrix generated by coded aperture and disperser in CASSI system as

$$\mathbf{H} = [\mathbf{D}_1, \dots, \mathbf{D}_{n_\lambda}] \in \mathbb{R}^{n_x(n_y+n_\lambda-1) \times n_x n_y n_\lambda}, \quad (7)$$

where, for $m = 1, \dots, n_\lambda$, $\mathbf{D}_m = \begin{bmatrix} \mathbf{0}^{(1)} \\ \mathbf{A}_m \\ \mathbf{0}^{(2)} \end{bmatrix} \in \mathbb{R}^{n_x(n_y+n_\lambda-1) \times n_x n_y}$, with $\mathbf{A}_m = \text{Diag}(\text{vec}(\mathbf{M})) \in \mathbb{R}^{n_x n_y \times n_x n_y}$ is a diagonal matrix and its diagonal element is $\text{vec}(\mathbf{M})$, $\mathbf{0}^{(1)} \in \mathbb{R}^{(m-1) \times n_x n_y}$ and $\mathbf{0}^{(2)} \in \mathbb{R}^{(n_\lambda-m) \times n_x n_y}$ represent the zero matrix. Finally, the vectorization expression of Eq. (3) is

$$\mathbf{y} = \mathbf{H}\mathbf{x} + \mathbf{z}. \quad (8)$$

After obtaining the measurement \mathbf{y} , the next task is to develop a decoding algorithm. Given \mathbf{y} and \mathbf{H} , solve \mathbf{x} .

2.2. Reconstruction Algorithms for SCI

SCI reconstruction algorithms mainly focus on how to solve the ill-posed inverse problem in (8), a.k.a., the reconstruction of SCI. Traditional methods are generally based on prior knowledge, which is used as a regularization condition to solve the problem, such as using total variation (TV) [3], sparsity [13], dictionary learning [1,67], non-local low rank [33], Gaussian mixture modes [59] etc. The main problem of these algorithms is that they need to manually set prior knowledge and iteratively solve the problem, and the reconstruction time is long and the quality is usually not good.

With its powerful learning capability, the neural network can directly learn a mapping relationship from the measurement to the original hyperspectral images, and the reconstruction speed can reach the millisecond level. End-to-end (E2E) deep learning methods (TSA-net [38], λ -net [41], SSI-ResU-Net [54]) take the measurement and masks as inputs, and use only a single network to reconstruct the desired signal directly. Plug-and-play (PnP) methods [27,69] use a pre-trained network as a denoiser plugged into iterative optimization [5,64]. Different from PnP methods, the denoising networks in each stage of the deep unfolding methods [37,55] are independent from each other, the parameters are not shared, and can be trained end-to-end like E2E methods.

Deep unfolding has the advantages of high-speed, high quality reconstruction and also enjoys the benefits of

physical-driven interpretability. Therefore, in this paper, we follow the deep unfolding framework [37], and propose a new deep denoiser block based on convolution and contextual transformer. The proposed module along with deep unfolding leads to SOTA results for SCI reconstruction.

2.3. Limitations of CNNs for Reconstruction

Due to the local connection and shift-invariance, the convolutional network [28] can extract the local features of the image very well, and is widely used in image recognition [18,23,26], object detection [45], semantic segmentation [36], image denoising [50] and other tasks [19,48]. However, its local connection property also makes it lack the ability of global perception. In order to improve the receptive field of convolution, deeper network architecture [18] or various pooling operations [22] are often used. Squeeze-and-excitation network (SENet) [22] uses the channel attention mechanism [52] to aggregate the global context and redistributes the weight to each channel. However, these methods generally lose a significant amount of detail information and are not friendly to image reconstruction and other tasks that need to recover local details.

Bearing the above concerns and considering the running time, we do not use very deep network structure in our work for the SCI reconstruction, and use convolution with a sliding step size of 2 to replace the traditional max pooling operation aiming to capture the local details of the desired spatio-spectral data-cube.

2.4. Visual Transformers

Vision Transformer (ViT) [11] and its variants [10,51,63,72] have verified the effectiveness of transformer architecture in computer vision tasks. However, training a good ViT model requires a large number of training datasets (*i.e.*, JFT-300M [49]), and its computational complexity increases quadratically with the image size. In order to better apply transformer to computer vision related tasks, the latest Swin transformer [34] proposes local window self attention mechanism and the shifting window method, which greatly reduces the computational complexity. The transformer network based on Swin has achieved amazing results in computer vision tasks such as image recognition [9], object detection [32], semantic segmentation [70,71] and image restoration [30], which further verifies the feasibility of transformer in computer vision. In addition, most transformers, including the Swin transformer, when calculating self attention, all the pairwise query-key are independently learned, and the rich contextual relationships between them are not used. Moreover, the self-attention mechanism in visual transformers often ignores local feature details, which is not conducive to low-level image tasks such as image reconstruction.

Inspired by contextual transformer (CoT) [29] and Con-

former networks [42], in this paper, we propose a network structure named CCoT, which can take advantage of convolution and transformer to extract more effective spectral features, and can be well applied to image reconstruction tasks such as SCI.

3. Proposed Network

In this section, we first briefly review the GAP-net [37] algorithm, which uses deep unfolding ideas [20] and generalized alternating projection (GAP) algorithm [31] for SCI reconstruction. We select GAP-net due to its high performance, robustness and flexibility for different SCI systems reported in [37]. Following this, we combine the advantages of convolution and transformer and then propose a module named convolution and contextual transformer, dubbed CCoT. We integrate this module into GAP-net to reconstruct hyperspectral images from the compressed measurement and masks.

3.1. Review of GAP-net for SCI Reconstruction

The SCI reconstruction algorithm is used to solve the following optimization problem:

$$\hat{\mathbf{x}} = \arg \min_{\mathbf{x}} \frac{1}{2} \|\mathbf{y} - \mathbf{H}\mathbf{x}\|^2 + \lambda\Omega(\mathbf{x}), \quad (9)$$

where the first term is the fidelity term and the second term, $\Omega(\mathbf{x})$, is the prior or regularization to confine the solutions. In GAP-net and other deep unfolding algorithms, implicit priors (represented by deep neural networks) have been used to improve the performance.

Following the framework of GAP, Eq. (9) can be rewritten as a constrained optimization problem by introducing an auxiliary parameter \mathbf{v} :

$$(\hat{\mathbf{x}}, \hat{\mathbf{v}}) = \arg \min_{\mathbf{x}, \mathbf{v}} \frac{1}{2} \|\mathbf{x} - \mathbf{v}\|_2^2 + \lambda\Omega(\mathbf{v}), \quad s.t. \quad \mathbf{y} = \mathbf{H}\mathbf{x}. \quad (10)$$

In order to solve Eq. (10), GAP decomposes it into the following subproblems for iterative solutions, where k denotes the iteration number.

- Solving \mathbf{x} : $\mathbf{x}^{(k+1)}$ is updated via an Euclidean projection of $\mathbf{v}^{(k)}$ on the linear manifold $\mathcal{M} : \mathbf{y} = \mathbf{H}\mathbf{x}$:

$$\mathbf{x}^{k+1} = \mathbf{v}^{(k)} + \mathbf{H}^\top (\mathbf{H}\mathbf{H}^\top)^{-1} (\mathbf{y} - \mathbf{H}\mathbf{v}^{(k)}). \quad (11)$$

- Solving \mathbf{v} : we can apply a trained denoiser to map \mathbf{x} closer to the desired signal space:

$$\mathbf{v}^{k+1} = \mathcal{D}_{k+1}(\mathbf{x}^{(k+1)}), \quad (12)$$

where $\mathcal{D}_{k+1}(\cdot)$ denotes the denoising operation.

It has been derived in the literature [64] that Eq. (11) has a closed-form solution due to the special structure of \mathbf{H} in Eq. (7). Therefore, the only difference and also the novelty is the denoising step in Eq. (12). In the following, we describe the novel CCoT block proposed in this work for efficient and effective SCI reconstruction. The general reconstruction framework is illustrated in Fig. 3 (a) and the detailed CCoT block is depicted in Fig. 3 (b-f).

3.2. Proposed CCoT Block for Deep Denoising

As mentioned in Section 2.4, to address the challenge of SCI reconstruction, we develop the CCoT block, where the convolution and transformer are used in parallel and can be well applied to image reconstruction tasks such as SCI.

Convolution Branch. As shown in Fig. 3 (b,e), the convolution branch consists of a down-sampling layer and a channel attention (CA) block. In this paper, we use convolution layer to perform down-sampling by sliding step s instead of the direct max pooling to capture fine details. The channel attention block draws lessons from the idea of SENet network [22], to automatically obtain the importance of each feature channel through learning, and then to improve the useful features according to this importance and suppress the features that are not significant for the current task. The first convolution layer and channel attention module are followed by a LeakyReLU activation function [58]. The proposed convolution branch can extract local features of image well.

Contextual Transformer Branch. By calculating the similarity between pixels, the traditional transformer makes the model focus on different regions and extract more effective features. However, when calculating paired query-key, they are relatively independent of each other. A single spectral image itself contains rich contextual information, and there is also a significant amount of correlation between adjacent spectra. Therefore, we designed a contextual transformer (CoT) branch to better obtain features of hyperspectral images.

As shown in Fig. 3 (b), CoT branch consists of a down-sampling layer and a CoT block. The structure of the down-sampling layer is the same as the convolution branch. As shown in Fig. 3 (f), we first recall that the input of the hyperspectral image is of $\mathbf{X}^0 \in \mathbb{R}^{n_x \times n_y \times n_\lambda}$, where n_x , n_y and n_λ represent the height, width and channel number of the spectral image, respectively. Then we define the queries, the keys, and the values as $\mathbf{K} \in \mathbb{R}^{n_x \times n_y \times n_\lambda}$, $\mathbf{Q} \in \mathbb{R}^{n_x \times n_y \times n_\lambda}$, $\mathbf{V} \in \mathbb{R}^{n_x \times n_y \times n_\lambda}$ respectively. Different from the traditional self-attention using 1×1 convolutions to generate mutually independent paired query-key, the CoT block first applies the group convolution of size $k \times k$ to generate a static key $\mathbf{K}^{(1)} \in \mathbb{R}^{n_x \times n_y \times n_\lambda}$ containing the context, and $\mathbf{K}^{(1)}$ can be used as a static context representation of input $\mathbf{X}^{(0)}$. \mathbf{Q} and \mathbf{V} can be generated by

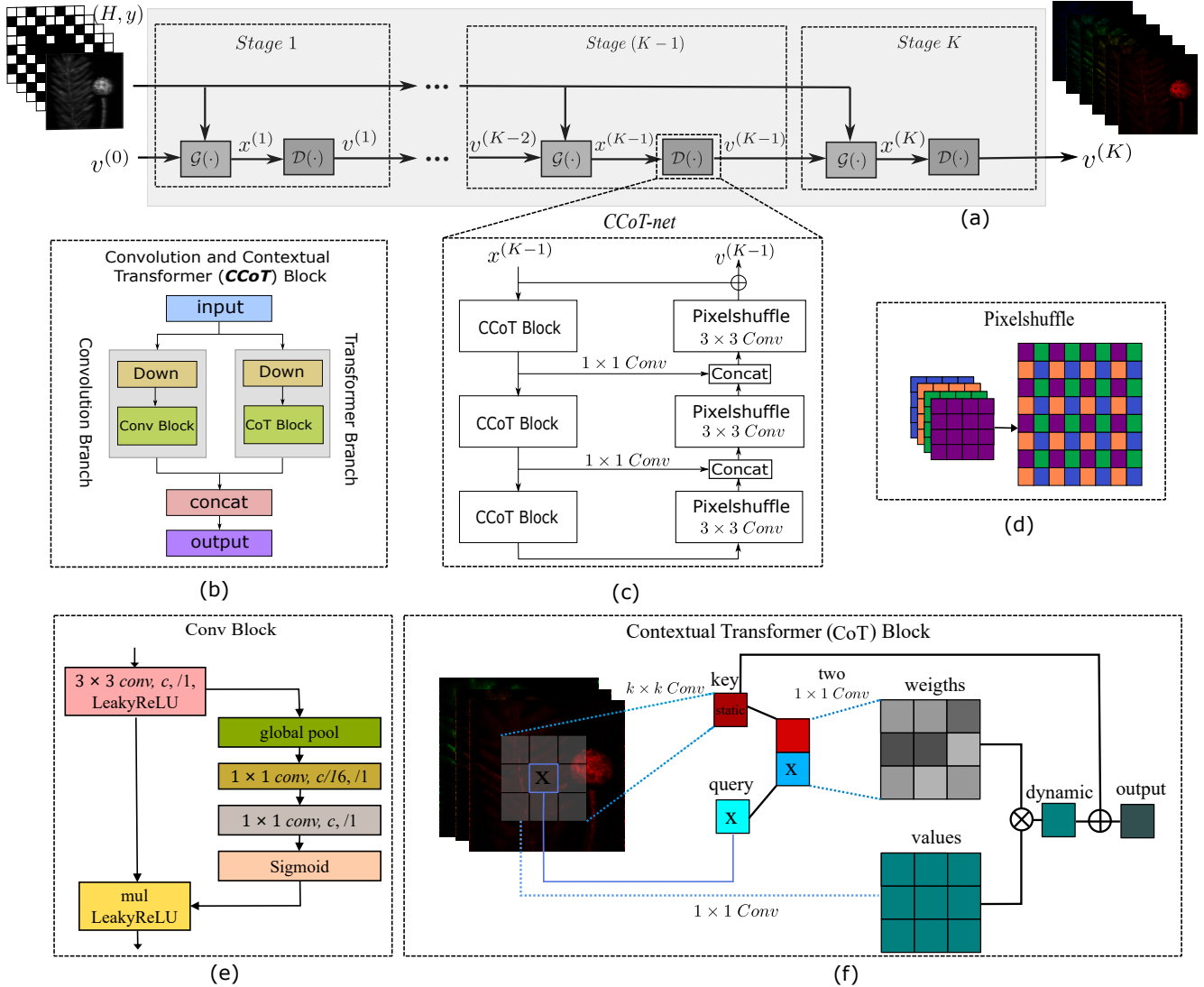


Figure 3. Architecture of the proposed GAP-CCoT. (a) GAP-net with K stages, $\mathcal{G}(\cdot)$ represents the operation of Eq. (11), $\mathcal{D}(\cdot)$ represents a denoiser and $v^{(0)} = \mathbf{H}^\top \mathbf{y}$. (b) Convolution branch and Transformer branch, The output is connected with concatenate. (c) CCoT-net, a denoiser of GAP algorithm. (d) Pixelshuffle algorithm for fast upsampling. (e) Convolution block with channel attention. (f) Contextual transformer block.

the traditional self-attention mechanism. Then, we concatenate $\mathbf{K}^{(1)}$ and \mathbf{Q} by the 3rd dimension (spectral channels), followed by two 1×1 convolutions to generate an attention matrix:

$$\mathbf{A} = \text{Conv}_\delta(\text{Conv}_\theta([\mathbf{K}^{(1)}, \mathbf{Q}]_3)), \quad (13)$$

where $[\]_3$ denotes the concatenation along the 3rd dimension, Conv_δ , Conv_θ represent two 1×1 convolutions, $\mathbf{A} \in \mathbb{R}^{n_x \times n_y \times (k^2 \times C_h)}$ represents the attention matrix containing context, C_h represents the number of attention heads. We use the traditional self-attention mechanism to perform a weighted summation of \mathbf{V} through \mathbf{A} to obtain the dynamic context $\mathbf{K}^{(2)} \in \mathbb{R}^{n_x \times n_y \times n_\lambda}$, and then fuse dynamic con-

text $\mathbf{K}^{(2)}$ and static context $\mathbf{K}^{(1)}$ as the output of the CoT block through the attention mechanism [22].

Finally, we concatenate the output of the convolution branch and the CoT branch as the final output of the CCoT block.

3.3. GAP-CCoT Network

As shown in Fig. 3 (c), we use CCoT module and pixelshuffle algorithm to construct a U-net [46] like network as the denoiser in the GAP-net. The network consists of a contracting path and an expansive path. *i)* The contracting path contains three CCoT modules and *ii)* the expansive path contains three upsampling modules. Each module of the

Table 1. The average PSNR in dB (upper entry in each cell) and SSIM (lower entry in each cell) of different algorithms on 10 synthetic datasets. Best results are in bold.

Algorithms	Scene1	Scene2	Scene3	Scene4	Scene5	Scene6	Scene7	Scene8	Scene9	Scene10	Average
TwIST [3]	24.81 0.730	19.99 0.632	21.14 0.764	30.30 0.874	21.68 0.688	22.16 0.660	17.71 0.694	22.39 0.682	21.43 0.729	22.87 0.595	22.44 0.703
GAP-TV [64]	25.13 0.724	20.67 0.630	23.19 0.757	35.13 0.870	22.31 0.674	22.90 0.635	17.98 0.670	23.00 0.624	23.36 0.717	23.70 0.551	23.73 0.683
DeSCI [33]	27.15 0.794	22.26 0.694	26.56 0.877	39.00 0.965	24.80 0.778	23.55 0.753	20.03 0.772	20.29 0.740	23.98 0.818	25.94 0.666	25.86 0.785
HSSP [55]	31.48 0.858	31.09 0.842	28.96 0.832	34.56 0.902	28.53 0.808	30.83 0.877	28.71 0.824	30.09 0.881	30.43 0.868	28.78 0.842	30.35 0.852
λ -net [41]	30.82 0.880	26.30 0.846	29.42 0.916	36.27 0.962	27.84 0.866	30.69 0.886	24.20 0.875	28.86 0.880	29.32 0.902	27.66 0.843	29.25 0.886
TSA-net [38]	31.26 0.887	26.88 0.855	30.03 0.921	39.90 0.964	28.89 0.878	31.30 0.895	25.16 0.887	29.69 0.887	30.03 0.903	28.32 0.848	30.15 0.893
PnP-DIP-HSI [40]	32.70 0.898	27.27 0.832	31.32 0.920	40.79 0.970	29.81 0.903	30.41 0.890	28.18 0.913	29.45 0.885	34.55 0.932	28.52 0.863	31.30 0.901
GAP-net [37]	33.03 0.921	29.52 0.903	33.04 0.940	41.59 0.972	30.95 0.924	32.88 0.927	27.60 0.921	30.17 0.904	32.74 0.927	29.73 0.901	32.13 0.924
DGSMP [24]	33.26 0.915	32.09 0.898	33.06 0.925	40.54 0.964	28.86 0.882	33.08 0.937	30.74 0.886	31.55 0.923	31.66 0.911	31.44 0.925	32.63 0.917
SSI-ResU-Net (v1) [54]	34.06 0.926	30.85 0.902	33.14 0.924	40.79 0.970	31.57 0.939	34.99 0.955	27.93 0.861	33.24 0.949	33.58 0.931	31.55 0.934	33.17 0.929
Ours	35.17 0.938	35.90 0.948	36.91 0.958	42.25 0.977	32.61 0.948	34.95 0.957	33.46 0.923	33.13 0.952	35.75 0.954	32.43 0.941	35.26 0.950

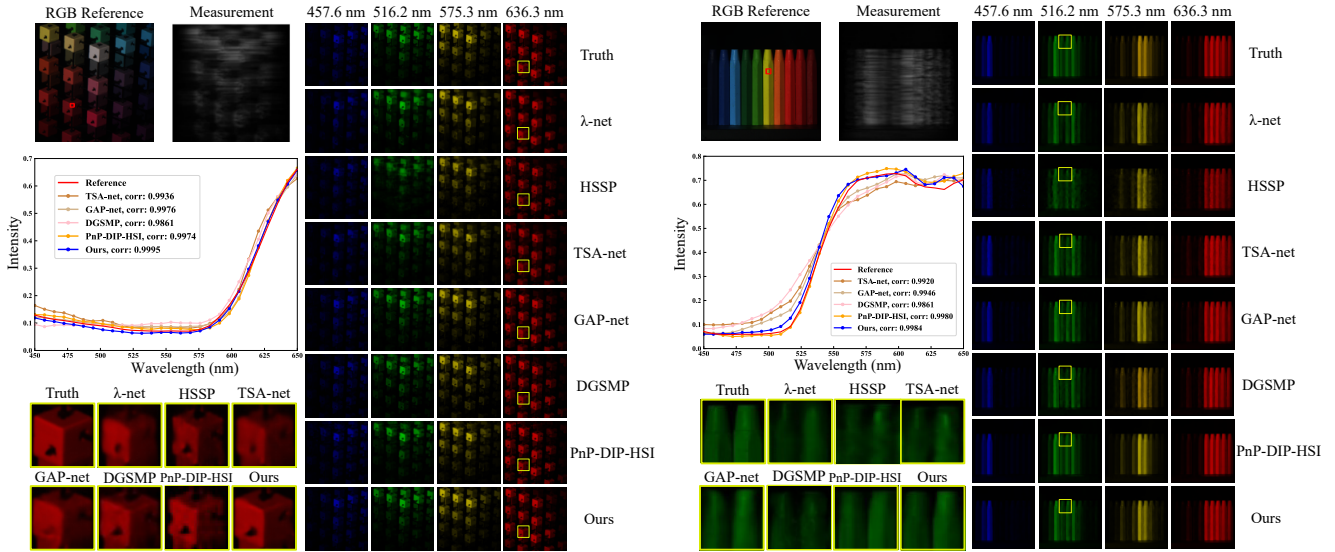


Figure 4. Reconstruction results of GAP-CSCoT and other spectral reconstruction algorithms (λ -net, HSSP, TSA-net, GAP-net, DGSMP, PnP-DIP-HSI) in Scene 3 (left) and Scene 9 (right). Zoom in for better view.

expansive path is first quickly upsampled by the pixelshuffle algorithm [47], and then followed by a 3×3 convolution, and finally concatenates the output from the corresponding stage of the contracting path (after a 1×1 convolution) as the input of the next module. Eventually, CCoT, GAP and deep unfolding form the reconstruction network (GAP-CCoT) of SCI.

Loss function. Lastly, the loss function of the proposed model is

$$\mathcal{L}_{MSE}(\Theta) = \frac{1}{n_\lambda} \sum_{n=1}^{n_\lambda} \|\hat{\mathbf{X}}_n - \mathbf{X}_n\|^2, \quad (14)$$

where $\mathcal{L}_{MSE}(\Theta)$ represents the Mean Square Error (MSE) loss, n_λ again represents the spectral channel to be reconstructed and $\hat{\mathbf{X}}_n \in \mathbb{R}^{n_x \times n_y}$ is the reconstructed hyperspectral image at the n -th spectral channel.

4. Experimental Results

In this section, we compare the performance of the proposed GAP-CCoT network with several SOTA methods on both simulation and real datasets. The peak-signal-to-noise-ratio (PSNR) and the the structured similarity index metrics

(SSIM) [56] are used to evaluate the performance of different HSI reconstruction methods.

4.1. Datasets

We use the hyperspectral dataset CAVE [62] for model training and KAIST [8] for model simulation testing. The CAVE dataset consists of 32 scenes, including full spectral resolution reflectance data from 400nm to 700nm with 10nm steps, and its spatial resolution is 512×512 . The KAIST dataset consists of 30 scenes with a spatial resolution of 2704×3376 . In order to match the wavelength of the real CASSI system, we follow the method proposed by TSA-net [38] and employ the spectral interpolation method to modify the training set and test data wavelength. The final wavelength was fitted to 28 spectral bands ranging from 450nm to 650nm.

4.2. Implementation Details

In the training process, we use random cropping, rotation, and flipping for the CAVE dataset augmentation. By simulating the imaging process of CASSI, we can obtain the corresponding measurement. We use measurement and mask as inputs to train the GAP-CCoT and use Adam optimizer [25] to optimize the model. The learning rate is set to be 0.001 initially and reduces by 10% every 10 epochs. Our model is trained for 200 epochs in total. All experiments are running on the NVIDIA RTX 8000 GPU using PyTorch.

Finally, we use a GAP-CCoT network with 9 stages as the reconstruction network, and no noise is added to the measurement during the training process for the simulation data. We added the shot noise to the measurements for the model training in the real data following the procedure in [37].

4.3. Simulation Results

We compared the method proposed in this paper with several SOTA methods (TwIST [3], GAP-TV [64], De-SCI [33], HSSP [55], λ -net [41], TSA-net [38], GAP-net [37], PnP-DIP-HSI [40], DGSMP [24] and SSI-ResU-Net (v1) [54]) on synthetic datasets. Table 1 shows the average PSNR and SSIM results of different spectral reconstruction algorithms. We can see that the average PSNR value of our proposed algorithm is 35.26 dB, the average SSIM value is 0.950. The average PSNR value is improved by 2.09 dB than the current best algorithm SSI-ResU-Net (v1, pre-printed, not published), and the SSIM value is improved by 0.021. In addition, compared with the self supervised learning method PnP-DIP-HSI and DGSMP method (best published results) based on the Maximum a Posterior (MAP) estimation, the average PSNR of the our proposed method is 3.96 dB and 2.63 dB higher, respectively. Based on these significant improvement, we can conduct the powerful learning capability of transformer and the proposed

Table 2. The average PSNR (left entry) and SSIM (right entry) results on synthetic with different masks.

Mask	PSNR, SSIM
Mask used in training	35.26, 0.950
New Mask1	35.10, 0.949
New Mask2	35.06, 0.948
New Mask3	35.06, 0.949
New Mask4	35.02, 0.948
New Mask5	34.99, 0.948

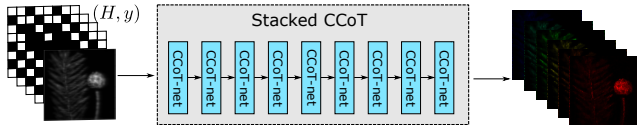


Figure 5. Architecture of the proposed Stacked CCoT. The input of the network is $H^T y$, the CCoT-net is the same as Fig. 3 (c)

CCoT block.

Fig. 4 shows part of the visualization results and spectral curves of two scenes using several SOTA spectral SCI reconstruction algorithms. Enlarging the local area, we can see that compared with other algorithms, our proposed method can recover more edge details and better spectral correlation.

4.4. Flexibility of GAP-CCoT to Mask Modulation

The CCoT-net only serves as a denoiser for the GAP algorithm, so the GAP-CCoT network proposed in this paper is thus flexible for different signal modulations. In order to verify this point, we train GAP-CCoT network on one mask and test on the other five different untrained masks. Table 2 shows the test results of the average PSNR value and SSIM value on 10 simulation data using different masks (5 new masks of size 256×256 randomly cropped from the real mask of size 660×660). We can observe that for a new mask that does not appear in training, the average PSNR decline is maintained within 0.27 dB, and the result is still better than other algorithms. Therefore, We can conclude that the GAP-CCoT network proposed in this paper is flexible for large-scale SCI reconstruction.

4.5. Ablation Study

Table 3. Ablation Study: The average PSNR and SSIM values by different algorithms on 10 synthetic data.

Algorithms	Stacked CCoT w/o CoT	GAP-CCoT w/o CoT	Stacked CCoT	GAP-CCoT
PSNR/SSIM	32.86, 0.924	34.13, 0.933	34.27, 0.936	35.26, 0.950

In order to verify the effectiveness of the contextual transformer and the GAP algorithm, we trained two different GAP-CCoT networks and two different Stacked CCoT networks (shown in Fig. 5) for spectral SCI reconstruction

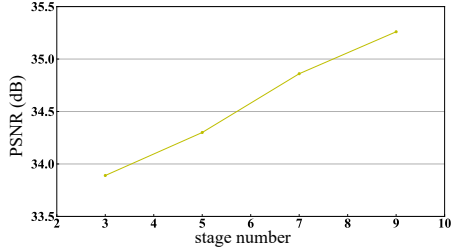


Figure 6. Effect of stage number on SCI reconstruction quality.

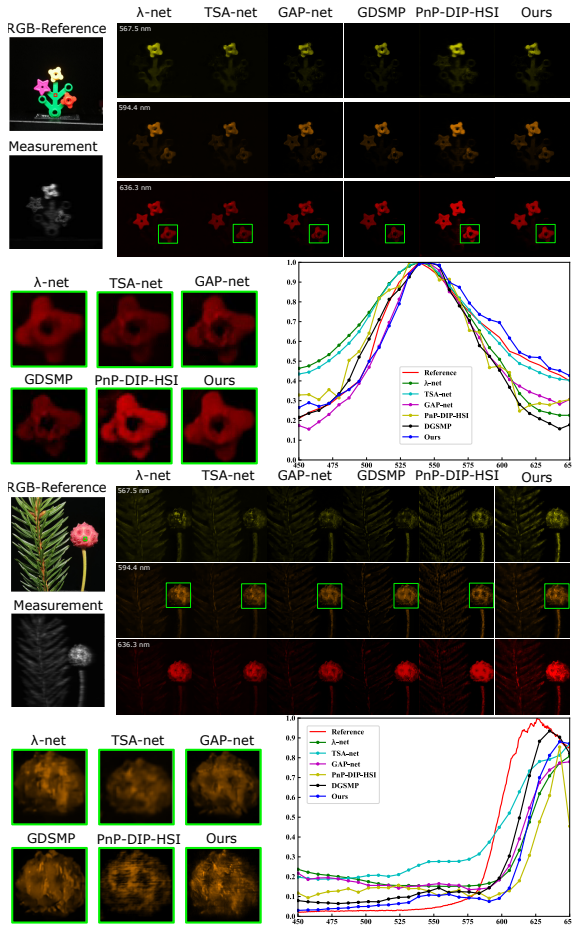


Figure 7. Reconstruction results of GAP-CCoT and other spectral reconstruction algorithms (λ -net, TSA-net, GAP-net, DGSMP, PnP-DIP-HSI) in two real scenes (Scene 1 and Scene 2).

respectively. Table 3 shows the reconstruction results of the two different networks we proposed, where ‘w/o’ CoT means removing the CoT branch at each stage of coding. We can clearly observe that the GAP-CCoT network is 0.99 dB higher in PSNR than the Stacked CCoT network. The PSNR value of the CoT module is improved by 1.13 dB and 1.41 dB on the GAP-CCoT network and the Stacked CCoT network respectively.

In order to verify the impact of the number of stages on the reconstruction quality, we trained multiple models with different number of stages. As can be seen from Fig. 6,

the model proposed in this paper only needs three stages to complete high reconstruction quality, and the reconstruction quality increases with the increase of the number of stages.

4.6. Real Data Results

We test the proposed method on several real data captured by CASSI system [53]. The system captures 28 spectral bands with wavelengths ranging from 450nm to 650nm. The spatial resolution of the object is 550×550 , and the spatial resolution of the measurements captured by the plane sensor is 550×604 . We compared our method with several SOTA methods (λ -net [41], TSA-net [38], GAP-net [37], PnP-DIP-HSI [40], DGSMP [24]) on real data. In addition to the results shown in Fig. 1, Fig. 7 shows part of the visualization results and spectral curves of the reconstructed real data of another scene. By zooming in on a local area, we can see that our proposed method can recover more details and fewer artifacts. In addition, from the spectral correlation curve, our proposed method also has higher spectral accuracy.

Table 4. Extending our method for **Video Compressive Sensing**: The average PSNR in dB, SSIM and running time per measurement of different algorithms on 6 benchmark datasets.

Algorithm	PSNR, SSIM	Running time(s)
GAP-TV [64]	26.73, 0.858	4.201 (CPU)
PnP-FFDNet [66]	29.70, 0.892	3.010 (GPU)
DeSCI [33]	32.65, 0.935	6180 (CPU)
BIRNAT [7]	33.31, 0.951	0.165 (GPU)
U-net [43]	29.45, 0.882	0.031 (GPU)
GAP-net-Unet-S12 [37]	32.86, 0.947	0.007 (GPU)
MetaSCI [57]	31.72, 0.926	0.025 (GPU)
RevSCI [6]	33.92, 0.956	0.190 (GPU)
Ours	33.53, 0.954	0.064 (GPU)

5. Conclusions and Discussion

In this paper, we use the inductive bias ability of convolution and the powerful modeling ability of transformer to propose a parallel module named CCoT, which can obtain more effective spectral features. We integrate this module with the deep unfolding idea and the GAP algorithm, which can be well applied to SCI reconstruction. In addition, we have also developed similar models for video compressive sensing [35, 65] and our model leads to excellent results, summarized in Table 4 and Fig. 8. We believe that by fine-tuning the proposed networks, we should be able to achieve state-of-the-art results for video compressive sensing and also other reconstruction tasks.

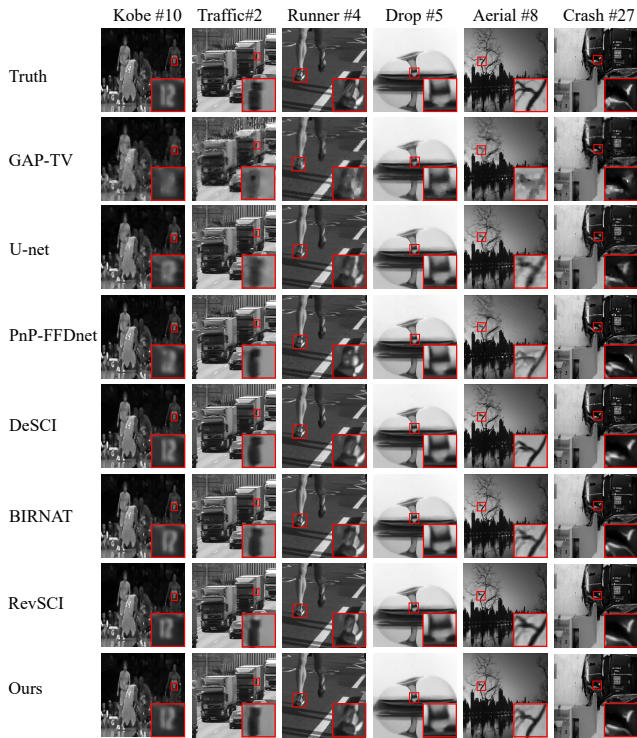


Figure 8. Reconstructed frame of our method and other algorithms (GAP-TV, DeSCI, PnP-FFDNet, U-net, BIRNAT, RevSCI) on 6 benchmark datasets.

References

- [1] Michal Aharon, Michael Elad, and Alfred Bruckstein. K-SVD: An algorithm for designing overcomplete dictionaries for sparse representation. *IEEE Transactions on signal processing*, 54(11):4311–4322, 2006. [3](#)
- [2] George Barbastathis, Aydogan Ozcan, and Guohai Situ. On the use of deep learning for computational imaging. *Optica*, 6(8):921–943, 2019. [2](#)
- [3] J M Bioucas-Dias and M A T Figueiredo. A new TwIST: Two-step iterative shrinkage/thresholding algorithms for image restoration. *IEEE Transactions on Image Processing*, 12(16):2992–3004, 2007. [2](#), [3](#), [6](#), [7](#)
- [4] José M Bioucas-Dias, Antonio Plaza, Gustavo Camps-Valls, Paul Scheunders, Nasser Nasrabadi, and Jocelyn Chanussot. Hyperspectral remote sensing data analysis and future challenges. *IEEE Geoscience and remote sensing magazine*, 1(2):6–36, 2013. [1](#)
- [5] Stephen Boyd, Neal Parikh, and Eric Chu. *Distributed optimization and statistical learning via the alternating direction method of multipliers*. Now Publishers Inc, 2011. [3](#)
- [6] Ziheng Cheng, Bo Chen, Guanliang Liu, Hao Zhang, Ruiying Lu, Zhengjue Wang, and Xin Yuan. Memory-efficient network for large-scale video compressive sensing. In *Proceedings of the IEEE/CVF Conference on Computer Vision and Pattern Recognition*, pages 16246–16255, 2021. [8](#)
- [7] Ziheng Cheng, Ruiying Lu, Zhengjue Wang, Hao Zhang, Bo Chen, Ziyi Meng, and Xin Yuan. BIRNAT: Bidirectional recurrent neural networks with adversarial training for video snapshot compressive imaging. In *European Conference on Computer Vision*, pages 258–275. Springer, 2020. [8](#)
- [8] Inchang Choi, Daniel S Jeon, Giljoo Nam, Diego Gutierrez, and Min H Kim. High-quality hyperspectral reconstruction using a spectral prior. *ACM Transactions on Graphics (TOG)*, 36(6):1–13, 2017. [7](#)
- [9] Jia Deng, Wei Dong, Richard Socher, Li-Jia Li, Kai Li, and Li Fei-Fei. Imagenet: A large-scale hierarchical image database. In *2009 IEEE conference on computer vision and pattern recognition*, pages 248–255. Ieee, 2009. [3](#)
- [10] Xiaoyi Dong, Jianmin Bao, Dongdong Chen, Weiming Zhang, Nenghai Yu, Lu Yuan, Dong Chen, and Baining Guo. CSWin transformer: A general vision transformer backbone with cross-shaped windows. *arXiv preprint arXiv:2107.00652*, 2021. [3](#)
- [11] Alexey Dosovitskiy, Lucas Beyer, Alexander Kolesnikov, Dirk Weissenborn, Xiaohua Zhai, Thomas Unterthiner, Mostafa Dehghani, Matthias Minderer, Georg Heigold, and Sylvain Gelly. An image is worth 16x16 words: Transformers for image recognition at scale. *arXiv preprint arXiv:2010.11929*, 2020. [3](#)
- [12] Yao-Ze Feng and Da-Wen Sun. Application of hyperspectral imaging in food safety inspection and control: a review. *Critical reviews in food science and nutrition*, 52(11):1039–1058, 2012. [1](#)
- [13] Mário A T Figueiredo, Robert D Nowak, and Stephen J Wright. Gradient projection for sparse reconstruction: Application to compressed sensing and other inverse problems. *IEEE Journal of selected topics in signal processing*, 1(4):586–597, 2007. [3](#)
- [14] Ying Fu, Tao Zhang, Lizhi Wang, and Hua Huang. Coded hyperspectral image reconstruction using deep external and internal learning. *IEEE Transactions on Pattern Analysis and Machine Intelligence*, 2021. [2](#)
- [15] Michael E Gehm, Renu John, David J Brady, Rebecca M Willett, and Timothy J Schulz. Single-shot compressive spectral imaging with a dual-disperser architecture. *Optics express*, 15(21):14013–14027, 2007. [1](#)
- [16] Karol Gregor and Yann LeCun. Learning fast approximations of sparse coding. In *Proceedings of the 27th international conference on international conference on machine learning*, pages 399–406, 2010. [2](#)
- [17] Kai Han, Yunhe Wang, Hanqing Chen, Xinghao Chen, Jianyuan Guo, Zhenhua Liu, Yehui Tang, An Xiao, Chun-jing Xu, Yixing Xu, et al. A survey on visual transformer. *arXiv preprint arXiv:2012.12556*, 2020. [2](#)
- [18] Kaiming He, Xiangyu Zhang, Shaoqing Ren, and Jian Sun. Deep residual learning for image recognition. In *Proceedings of the IEEE conference on computer vision and pattern recognition*, pages 770–778, 2016. [3](#)
- [19] Lingxiao He, Xingyu Liao, Wu Liu, Xinchun Liu, Peng Cheng, and Tao Mei. Fastreid: A pytorch toolbox for general instance re-identification. *arXiv preprint arXiv:2006.02631*, 2020. [3](#)
- [20] John R Hershey, Jonathan Le Roux, and Felix Weninger. Deep unfolding: Model-based inspiration of novel deep architectures. *arXiv preprint arXiv:1409.2574*, 2014. [4](#)

- [21] Y. Hitomi, J. Gu, M. Gupta, T. Mitsunaga, and S. K. Nayar. Video from a single coded exposure photograph using a learned over-complete dictionary. In *2011 International Conference on Computer Vision*, pages 287–294, Nov 2011. [2](#)
- [22] Jie Hu, Li Shen, and Gang Sun. Squeeze-and-excitation networks. In *Proceedings of the IEEE conference on computer vision and pattern recognition*, pages 7132–7141, 2018. [3](#), [4](#), [5](#)
- [23] Gao Huang, Zhuang Liu, Laurens Van Der Maaten, and Kilian Q Weinberger. Densely connected convolutional networks. In *Proceedings of the IEEE conference on computer vision and pattern recognition*, pages 4700–4708, 2017. [3](#)
- [24] Tao Huang, Weisheng Dong, Xin Yuan, Jinjian Wu, and Guangming Shi. Deep gaussian scale mixture prior for spectral compressive imaging. In *Proceedings of the IEEE/CVF Conference on Computer Vision and Pattern Recognition*, pages 16216–16225, 2021. [1](#), [6](#), [7](#), [8](#)
- [25] Diederik P Kingma and Jimmy Ba. Adam: A method for stochastic optimization. *arXiv preprint arXiv:1412.6980*, 2014. [7](#)
- [26] Alex Krizhevsky, Ilya Sutskever, and Geoffrey E Hinton. Imagenet classification with deep convolutional neural networks. *Advances in neural information processing systems*, 25:1097–1105, 2012. [3](#)
- [27] Zeqiang Lai, Kaixuan Wei, and Ying Fu. Deep plug-and-play prior for hyperspectral image restoration. *Neurocomputing*, 2022. [3](#)
- [28] Yann LeCun, Yoshua Bengio, et al. Convolutional networks for images, speech, and time series. *The handbook of brain theory and neural networks*, 3361(10):1995, 1995. [3](#)
- [29] Yehao Li, Ting Yao, Yingwei Pan, and Tao Mei. Contextual transformer networks for visual recognition. *arXiv preprint arXiv:2107.12292*, 2021. [3](#)
- [30] Jingyun Liang, Jiezhang Cao, Guolei Sun, Kai Zhang, Luc Van Gool, and Radu Timofte. SwinIR: Image restoration using swin transformer. In *Proceedings of the IEEE/CVF International Conference on Computer Vision*, pages 1833–1844, 2021. [3](#)
- [31] Xuejun Liao, Hui Li, and Lawrence Carin. Generalized alternating projection for weighted- $\ell_{2,1}$ minimization with applications to model-based compressive sensing. *SIAM Journal on Imaging Sciences*, 7(2):797–823, 2014. [4](#)
- [32] Tsung-Yi Lin, Michael Maire, Serge Belongie, James Hays, Pietro Perona, Deva Ramanan, Piotr Dollár, and C Lawrence Zitnick. Microsoft COCO: Common objects in context. In *European conference on computer vision*, pages 740–755. Springer, 2014. [3](#)
- [33] Yang Liu, Xin Yuan, Jinli Suo, David J Brady, and Qionghai Dai. Rank minimization for snapshot compressive imaging. *IEEE transactions on pattern analysis and machine intelligence*, 41(12):2990–3006, 2018. [2](#), [3](#), [6](#), [7](#), [8](#)
- [34] Ze Liu, Yutong Lin, Yue Cao, Han Hu, Yixuan Wei, Zheng Zhang, Stephen Lin, and Baining Guo. Swin transformer: Hierarchical vision transformer using shifted windows. *arXiv preprint arXiv:2103.14030*, 2021. [3](#)
- [35] Patrick Lull, Xuejun Liao, Xin Yuan, Jianbo Yang, David Kittle, Lawrence Carin, Guillermo Sapiro, and David J Brady. Coded aperture compressive temporal imaging. *Optics express*, 21(9):10526–10545, 2013. [2](#), [8](#)
- [36] Jonathan Long, Evan Shelhamer, and Trevor Darrell. Fully convolutional networks for semantic segmentation. In *Proceedings of the IEEE conference on computer vision and pattern recognition*, pages 3431–3440, 2015. [3](#)
- [37] Ziyi Meng, Shirin Jalali, and Xin Yuan. GAP-net for snapshot compressive imaging. *arXiv preprint arXiv:2012.08364*, 2020. [1](#), [2](#), [3](#), [4](#), [6](#), [7](#), [8](#)
- [38] Ziyi Meng, Jiawei Ma, and Xin Yuan. End-to-end low cost compressive spectral imaging with spatial-spectral self-attention. In *European Conference on Computer Vision*, pages 187–204. Springer, 2020. [3](#), [6](#), [7](#), [8](#)
- [39] Ziyi Meng, Mu Qiao, Jiawei Ma, Zhenming Yu, Kun Xu, and Xin Yuan. Snapshot multispectral endomicroscopy. *Optics Letters*, 45(14):3897–3900, 2020. [1](#)
- [40] Ziyi Meng, Zhenming Yu, Kun Xu, and Xin Yuan. Self-supervised neural networks for spectral snapshot compressive imaging. In *Proceedings of the IEEE/CVF International Conference on Computer Vision*, pages 2622–2631, 2021. [1](#), [2](#), [6](#), [7](#), [8](#)
- [41] Xin Miao, Xin Yuan, Yunchen Pu, and Vassilis Athitsos. λ -net: Reconstruct hyperspectral images from a snapshot measurement. In *Proceedings of the IEEE/CVF International Conference on Computer Vision*, pages 4059–4069, 2019. [2](#), [3](#), [6](#), [7](#), [8](#)
- [42] Zhiliang Peng, Wei Huang, Shanzhi Gu, Lingxi Xie, Yaowei Wang, Jianbin Jiao, and Qixiang Ye. Conformer: Local features coupling global representations for visual recognition. *arXiv preprint arXiv:2105.03889*, 2021. [4](#)
- [43] Mu Qiao, Ziyi Meng, Jiawei Ma, and Xin Yuan. Deep learning for video compressive sensing. *APL Photonics*, 5(3):30801, 2020. [8](#)
- [44] D. Reddy, A. Veeraraghavan, and R. Chellappa. P2c2: Programmable pixel compressive camera for high speed imaging. In *CVPR 2011*, pages 329–336, June 2011. [2](#)
- [45] Joseph Redmon, Santosh Divvala, Ross Girshick, and Ali Farhadi. You only look once: Unified, real-time object detection. In *Proceedings of the IEEE conference on computer vision and pattern recognition*, pages 779–788, 2016. [3](#)
- [46] Olaf Ronneberger, Philipp Fischer, and Thomas Brox. U-Net: Convolutional networks for biomedical image segmentation. In *International Conference on Medical image computing and computer-assisted intervention*, pages 234–241. Springer, 2015. [2](#), [5](#)
- [47] Wenzhe Shi, Jose Caballero, Ferenc Huszár, Johannes Totz, Andrew P Aitken, Rob Bishop, Daniel Rueckert, and Zehan Wang. Real-time single image and video super-resolution using an efficient sub-pixel convolutional neural network. In *Proceedings of the IEEE conference on computer vision and pattern recognition*, pages 1874–1883, 2016. [6](#)
- [48] Robert Stone et al. Centertrack: An ip overlay network for tracking dos floods. In *USENIX Security Symposium*, volume 21, page 114, 2000. [3](#)
- [49] Chen Sun, Abhinav Shrivastava, Saurabh Singh, and Abhinav Gupta. Revisiting unreasonable effectiveness of data in deep learning era. In *Proceedings of the IEEE international conference on computer vision*, pages 843–852, 2017. [3](#)

- [50] Chunwei Tian, Lunke Fei, Wenxian Zheng, Yong Xu, Wangmeng Zuo, and Chia-Wen Lin. Deep learning on image denoising: An overview. *Neural Networks*, 2020. 3
- [51] Hugo Touvron, Matthieu Cord, Matthijs Douze, Francisco Massa, Alexandre Sablayrolles, and Hervé Jégou. Training data-efficient image transformers & distillation through attention. In *International Conference on Machine Learning*, pages 10347–10357. PMLR, 2021. 3
- [52] Ashish Vaswani, Noam Shazeer, Niki Parmar, Jakob Uszkoreit, Llion Jones, Aidan N Gomez, Łukasz Kaiser, and Illia Polosukhin. Attention is all you need. In *Advances in neural information processing systems*, pages 5998–6008, 2017. 3
- [53] Ashwin Wagadarikar, Renu John, Rebecca Willett, and David Brady. Single disperser design for coded aperture snapshot spectral imaging. *Applied optics*, 47(10):B44–B51, 2008. 1, 2, 8
- [54] Jiamian Wang, Yulun Zhang, Xin Yuan, Yun Fu, and Zhiqiang Tao. A new backbone for hyperspectral image reconstruction. *arXiv preprint arXiv:2108.07739*, 2021. 2, 3, 6, 7
- [55] Lizhi Wang, Chen Sun, Ying Fu, Min H Kim, and Hua Huang. Hyperspectral image reconstruction using a deep spatial-spectral prior. In *Proceedings of the IEEE/CVF Conference on Computer Vision and Pattern Recognition*, pages 8032–8041, 2019. 2, 3, 6, 7
- [56] Zhou Wang, Alan C Bovik, Hamid R Sheikh, and Eero P Simoncelli. Image quality assessment: from error visibility to structural similarity. *IEEE transactions on image processing*, 13(4):600–612, 2004. 7
- [57] Zhengjue Wang, Hao Zhang, Ziheng Cheng, Bo Chen, and Xin Yuan. MetaSCI: Scalable and adaptive reconstruction for video compressive sensing. In *Proceedings of the IEEE/CVF Conference on Computer Vision and Pattern Recognition*, pages 2083–2092, 2021. 8
- [58] Bing Xu, Naiyan Wang, Tianqi Chen, and Mu Li. Empirical evaluation of rectified activations in convolutional network. *arXiv preprint arXiv:1505.00853*, 2015. 4
- [59] Jianbo Yang, Xuejun Liao, Xin Yuan, Patrick Lull, David J Brady, Guillermo Sapiro, and Lawrence Carin. Compressive sensing by learning a Gaussian mixture model from measurements. *IEEE Transactions on Image Processing*, 24(1):106–119, 2014. 3
- [60] Yan Yang, Jian Sun, Huibin Li, and Zongben Xu. Deep admm-net for compressive sensing mri. In *Proceedings of the 30th international conference on neural information processing systems*, pages 10–18, 2016. 2
- [61] Yan Yang, Jian Sun, Huibin Li, and Zongben Xu. Admmcnet: A deep learning approach for image compressive sensing. *IEEE transactions on pattern analysis and machine intelligence*, 42(3):521–538, 2018. 2
- [62] Fumihito Yasuma, Tomoo Mitsunaga, Daisuke Iso, and Shree K Nayar. Generalized assorted pixel camera: post-capture control of resolution, dynamic range, and spectrum. *IEEE transactions on image processing*, 19(9):2241–2253, 2010. 7
- [63] Li Yuan, Yunpeng Chen, Tao Wang, Weihao Yu, Yujun Shi, Francis E H Tay, Jiashi Feng, and Shuicheng Yan. Tokens-to-token ViT: Training vision transformers from scratch on imageNet. *arXiv e-prints*, pages arXiv–2101, 2021. 3
- [64] Xin Yuan. Generalized alternating projection based total variation minimization for compressive sensing. In *2016 IEEE International Conference on Image Processing (ICIP)*, pages 2539–2543. IEEE, 2016. 2, 3, 4, 6, 7, 8
- [65] Xin Yuan, David J Brady, and Aggelos K Katsaggelos. Snapshot compressive imaging: Theory, algorithms, and applications. *IEEE Signal Processing Magazine*, 38(2):65–88, 2021. 2, 8
- [66] Xin Yuan, Yang Liu, Jinli Suo, and Qionghai Dai. Plug-and-play algorithms for large-scale snapshot compressive imaging. In *Proceedings of the IEEE/CVF Conference on Computer Vision and Pattern Recognition*, pages 1447–1457, 2020. 8
- [67] Xin Yuan, Tsung-Han Tsai, Ruoyu Zhu, Patrick Lull, David Brady, and Lawrence Carin. Compressive hyperspectral imaging with side information. *IEEE Journal of selected topics in Signal Processing*, 9(6):964–976, 2015. 3
- [68] Jian Zhang and Bernard Ghanem. Ista-net: Interpretable optimization-inspired deep network for image compressive sensing. In *Proceedings of the IEEE conference on computer vision and pattern recognition*, pages 1828–1837, 2018. 2
- [69] Siming Zheng, Yang Liu, Ziyi Meng, Mu Qiao, Zhishen Tong, Xiaoyu Yang, Shensheng Han, and Xin Yuan. Deep plug-and-play priors for spectral snapshot compressive imaging. *Photonics Research*, 9(2):B18–B29, 2021. 3
- [70] Bolei Zhou, Hang Zhao, Xavier Puig, Sanja Fidler, Adela Barriuso, and Antonio Torralba. Scene parsing through ADE20K dataset. In *Proceedings of the IEEE conference on computer vision and pattern recognition*, pages 633–641, 2017. 3
- [71] Bolei Zhou, Hang Zhao, Xavier Puig, Tete Xiao, Sanja Fidler, Adela Barriuso, and Antonio Torralba. Semantic understanding of scenes through the ADE20K dataset. *International Journal of Computer Vision*, 127(3):302–321, 2019. 3
- [72] Xizhou Zhu, Weijie Su, Lewei Lu, Bin Li, Xiaogang Wang, and Jifeng Dai. Deformable DETR: Deformable transformers for end-to-end object detection. In *International Conference on Learning Representations*, 2020. 3